STRUCTURAL AND CHARACTERIZATION OF PHOTOCONDUCTIVE TELLUROVANADATE GLASSES WITH LITHIUM OXIDE FOR OPTOELECTRONIC DEVICES

I. M. ASHRAF[a,b], M. FAROUK[c], F. AHMAD[d], M. M. EL OKR[c],
M. M. ABDEL–AZIZ[c], E. S. YOUSEF[a,e*]
[a]*Physics Dep., Faculty of Science, King Khalid University, P. O. Box 9004, Abha, Saudi Arabia*
[b]*Physics Dep., Faculty of Sciences, Aswan University, Aswan, Egypt*
[c]*Physics Department, Faculty of Science, Al- Azahr University, Nasr city, Cairo, Egypt*
[d]*Physics Department, Faculty of Science, Al- Azahr University (Girls Branch), Nasr City, Cairo, Egypt*
[e]*Physics Department, Faculty of Science, Al- Azahr University, Assiut Branch, Egypt*

In this work, $(90 - x)$ $TeO_2 - (x)V_2O_5 - 10Li_2O$ glass for (x = 20, 30, 40, 50, 60 and 70 in mol %) were prepared by rapid quenching technique. The properties of semiconducting glasses and information about the behavior of the photo excitation were tested by measuring the steady-state and transient photoconductivity. Also, the mechanisms of a conductivity type, electronic, ionic, or mixed electronic-ionic conduction were discussed. The photoconductivity measurements show that the photocurrent not only increased with rising light intensity but also by increasing vanadium pentoxide and a decrease of tellurium dioxide. The transient photoconductivity behavior in glass materials was performed via three sets of measurements for the rise and decay of photocurrent at different intensities, temperatures and applied voltages. The exponent parameter γ that determines the recombination mechanism in the semiconductor materials lies between 0.47 and 0.59 which can be considered a continuous distribution of traps exists in the band gap region with predominant bimolecular carrier recombination in the glass samples. The activation energy values of the present samples were lying between 0.314 and 0.249 eV in dark, while in the photo, they changed to 0.275 and 0.213 eV.

1. Introduction

Oxide glasses containing transition metals have been studied because of their semiconducting properties [1-3]. These glasses have been important usefulness due to of their technical application, specifically optical and electrical memory switching, cathode materials [4], optoelectronic devices such as fiber Raman amplifiers [5], and waveguide devices [6]. Electric properties of tellurite glasses containing transition metal oxide (TMO) have been examined due to their potential use in solid-state devices. The addition of TMO makes them electronic or mixed electronic-ionic conductors, which are potential interest as cathode materials for solid-state battery [7]. Tellurite glasses containing a large amount of V_2O_5 have high electrical conductivity, as compared with vanadium phosphate glasses or other glasses containing metal oxides with the same amount of charge carriers [8]. Tellurovanadate glasses having semiconducting nature which is assigned to vanadium ions have two valence states and the electrical conductivity is activated by hopping from the low valence state to the high valence state (between V^{4+} and V^{5+} ions sites) [9-11]. The addition of alkali oxides like Li_2O, Na_2O, or K_2O to the glass forming oxides such as

---

TeO_2 and P_2O_5, ionic conductivity exhibits due to the movement of alkali ions [12-14]. While the addition of TMO and alkali metals oxide to the oxide glass, exhibits Mixed of ionic-electronic conduction [15,16], such as $Ag_2O - V_2O_5 - TeO_2$ [17], $Li_2O - V_2O_5 - TeO_2$ [18] $Li_2O - V_2O_5 - P_2O_5$ and $Na_2O - V_2O_5 - P_2O_5$ [19].

Jayasinghe el al. [20] reported on the change of conduction mechanism from electronic to ionic in $3TeO_2 - xLi_2O - (1-x) V_2O_5$ glasses at x = 0.5. Montani et al. [21] observed the mixed electronic – ionic conduction in $xLi_2O - (1-x) V_2O_5 - 2TeO_2$ glasses and the transition from electronic to ionic conduction for x = 0.6. Krins et al. [22] showed that, for $xLi_2O - (1-x) [0.3V_2O_5 - 0.7TeO_2]$ glass, electronic to ionic transition was observed around 20 – 30 mol% Li_2O. In the electronic region, the decrease of conductivity due to the relative opening of glass network as a result of the creation of nonbridging oxygens (NBOs) which increases the distance between polaron hopping sites [18, 22].

Photoconductivity is a profitable tool to study the properties of semiconducting glasses. It is an important tool for provides information about the behavior of the photo – excitations. The conductivity of the material depends on the carrier density and process of carrier generation, trapping and recombination.

Photocurrent measurements in chalcogenide semiconducting glasses depend on illumination intensity and on temperature permits the identification of monomolecular or bimolecular recombination. The structure and bonding configuration of chalcogenide glasses changes with light incidence, this due to rapid localization of the photoexcited carriers. Rise and decay of photocurrent in transient photoconductivity measurements shows the existence of traps in the mobility gap in materials. These traps originate from the defect states existing in the materials. Transient photoconductivity measurements give information about the localized states in these materials. Transient photoconductivity measurements have been reported earlier by various workers [23-25].

The present paper reports on the experimental results of steady-state and transient photoconductivity measurements in amorphous $[(90 - x) TeO_2 - (x)V_2O_5 - 10Li_2O]$ where (x = 20, 30, 40, 50, 60 and 70 mol%) prepared by rapid quenching technique, and explain the mechanism of conductivity type, electronic, ionic, or mixed electronic – ionic conduction.

2. Experimental techniques

2.1. Glass preparation

The ternary tellurovanadate glass samples with starting composition of $[(90 - x) TeO_2 - (x)V_2O_5 - 10Li_2O]$ where (x = 20, 30, 40, 50, 60 and 70 mol%) were prepared by mixing specified weights of vanadium pentoxide (V_2O_5, 99.6% purity, Sigma Aldrich), tellurium dioxide (TeO_2, 99.99% purity, Alfa Aesar), and lithium oxide (Li_2O, 97% purity, Sigma Aldrich). All samples were prepared using the melt-quenching technique. An appropriate amount of TeO_2, V_2O_5, and Li_2O powder was mixed in a platinum crucible. The 20 g batches of the mixture were preheated at a temperature of 980 ^{o}C in a furnace for 40 min to improve homogeneity. After that, the samples transferred to another furnace to be quenched on molds of stainless steel for annealing process at 220 ^{o}C for 2 hrs, then the furnace was switched off and the samples were allowed to cool.

2.2. Photoconductivity measurements

The sample used in the photoelectric measurements was mounted on the cold finger inside a cryostat (LN Oxford DN1704 – type). A digital temperature controller (Oxford ITC601 – type) controlled the temperature inside the cryostat. The contacts between the samples and the metal electrodes were made using silver paste. Excitation was done by a tungsten lamp of 1000 W, which was connected to a variance for adjusting the light intensity at the sample surface. Using an optical system consisting of two convex lenses, the light was focused onto the sample making sure that the region between the two electrodes was homogeneously illuminated. Moreover, the heat radiation from the light source was avoided by passing the light beam through a water filter. Fig. 1 show the experimental arrangement used by steady-state and transient photoconductivity

measurement. The programmable digital electrometer (Keithley 6517B), was used to control the voltage applied to the samples and measure the current. The net photocurrent was obtained by subtracting the dark current from the measured photocurrent. The total current (in the presence of light), at each point, was recorded after reaching a steady – state value. The program 6517 Hi-R Step Response was used in transient photoconductivity measurement, which allows us to adjust the duration of measure.
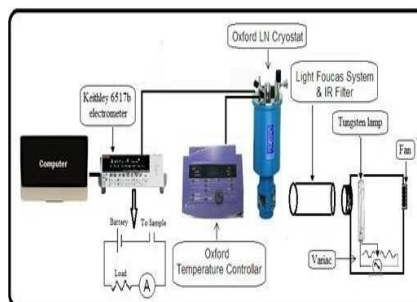
Fig. 1. Schematic Diagram of the Experimental Arrangements used in the Photoconductivity Measurements.

3. Results and discussion

The dependence of the current density (J) on applied electric field (E) in the absence and presence the white light for the glass materials [(90 – x) TeO_2 – (x)V_2O_5 – 10Li_2O] are studied at room temperature. The behavior of steady photocurrent density with the electric field at dark and different illumination intensities varying from 129 – 4300 lux, are shown in Fig. (2). All samples show a similar trend, where the straight lines passing through the origin confirm the ohmic nature of the electrical contacts for the present samples. It has been observed from the results that the increase in photocurrent not only with increasing light intensity but also with increasing vanadium pentoxide with a decrease in tellurium dioxide. The increase in photocurrent leads to an increase in photoconductivity as a result of the increase in the percentage of vanadium pentoxide continues until the percentage of it reached 60 mol%. If the vanadium pentoxide continues exceeds 60 mol%, there is a decrease in photoconductivity as shown in Table (1). The semiconducting behavior of the transition metal oxide glasses is believed to arise from the hopping of small polarons from the ions of low valence state to the ions of high valence state [26]. Then, it can be proposed that, the conduction in the glass system [(90 – x) TeO_2 – (x)V_2O_5 – 10Li_2O] in terms of hopping of electrons between localized states (from the lower valence state V^{4+} to the highest state V^{5+}). The increase in conductivity by increasing of V_2O_5 up to 60 mol%, after that, the conductivity decreases by increasing the content of V_2O_5 exceeds 60 mol%, suggests that the behavior of conductivity is related to mixed electronic – ionic conductivity where the presence of Li^+ is blocked by the presence of vanadium ions, then resulting in an increase in photoconductivity. And the Li^+ ions have high mobility than vanadium ions may result in a decrease in photoconductivity with increase V_2O_5 exceeds 60 mol%. Sega et al. [27] showed that, in the binary system xV_2O_5 – (1-x) TeO_2, the increase in vanadium content results in a decrease of R_V (vanadium ion spacing) distance, which simplifies electron hopping from V^{4+} to V^{5+} sites. When V_2O_5 added in higher content (> 60 mol%), the creation of NBOs, due to the gradual transformation from VO_5 to VO_4 structural units. This structure is more open for ion motion and the conditions for electronic hopping are less suitable which leads to a decrease in conductivity. Then, the glass composition $30TeO_2$ – $60V_2O_5$ – $10Li_2O$ may be explained as a transit point between electronic and ionic conduction. The behavior of transition from the electronic conduction to the ionic conduction was reported earlier for some other glass systems [28,29]. The decrease of electronic conductivity and the increase of the ionic one due to the changes in glass composition studied by Bih et al. [30] for the glass system Li_2O – V_2O_5 – P_2O_5.

330
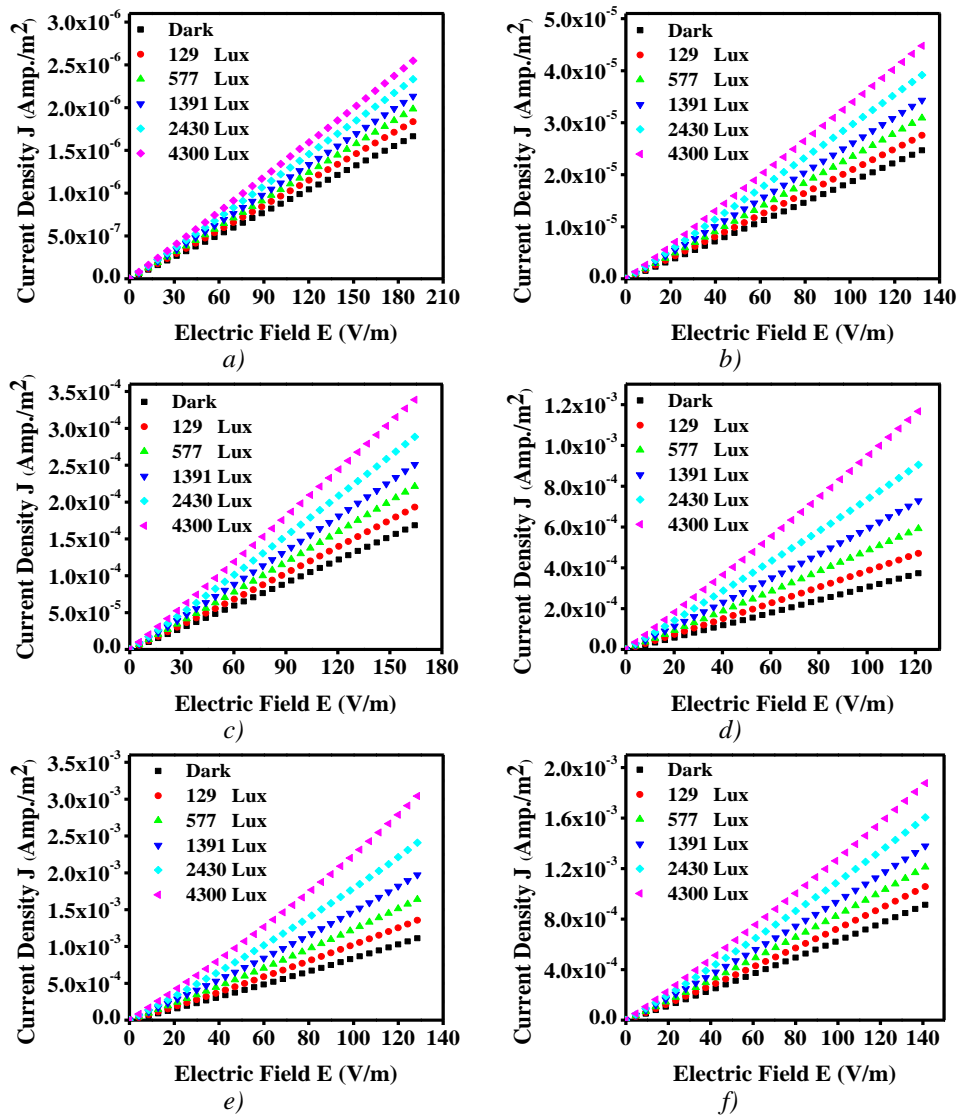
Fig. 2. Variation of Electric Field with Current Density for (a) $70TeO_2 – 20V_2O_5 – 10Li_2O$, (b) $60TeO_2 – 30V_2O_5 – 10Li_2O$, (c) $50TeO_2 – 40V_2O_5 – 10Li_2O$, (d) $40TeO_2 – 50V_2O_5 – 10Li_2O$, (e) $30TeO_2 – 60V_2O_5 – 10Li_2O$, (f) $20TeO_2 – 70V_2O_5 – 10Li_2O$ Glass Materials.

Table 1. Photoconductivity and Photosensitivity at various intensities in $[(90 – x) TeO_2 – (x)V_2O_5 – 10Li_2O]$ Glass Materials.

Glass Materials	Photoconductivity x10^{-9} $(\Omega.cm)^{-1}$						Photosensitivity				
	0 lux	129 lux	577 lux	1391 lux	2430 lux	4300 lux	129 lux	577 lux	1391 lux	2430 lux	4300 lux
$70TeO_2 – 20V_2O_5 – 10Li_2O$	8.793	0.9029	1.682	2.474	3.514	4.632	0.103	0.191	0.281	0.399	0.527
$60TeO_2 – 30V_2O_5 – 10Li_2O$	187.5	21.72	46.93	72.90	110.1	152.5	0.116	0.25	0.389	0.587	0.813
$50TeO_2 – 40V_2O_5 – 10Li_2O$	1029	149.4	322.1	501.0	734.2	1038	0.145	0.313	0.487	0.714	1.009
$40TeO_2 – 50V_2O_5 – 10Li_2O$	3090	804.0	1798	2910	4354	6513	0.260	0.582	0.942	1.408	2.107
$30TeO_2 – 60V_2O_5 – 10Li_2O$	8698	1906	4032	6594	9940	14760	0.219	0.464	0.758	1.143	1.697
$20TeO_2 – 70V_2O_5 – 10Li_2O$	6509	1020	2101	3267	4874	6790	0.157	0.323	0.502	0.749	1.043

The densities of both types of charge carriers (N_V and N_{Li}), and the ion spacing (R_V and R_{Li}) as shown in the Table 2. To obtain the transition metal ion spacing, the V ion and Li ion densities firstly calculated [31] using the formula;

$$N_{V-ion} = 2\left[\left(\frac{\rho x_{V_2O_5}}{M_{V_2O_5}}\right)N_A\right] \tag{1}$$

$$N_{Li-ion} = 2\left[\left(\frac{\rho x_{Li_2O}}{M_{Li_2O}}\right)N_A\right] \tag{2}$$

where ρ is the glass density, x_i is the mole fraction of V_2O_5 or Li_2O, M_i is the molecular weight of V_2O_5 or Li_2O and N_A is the Avogadro's number. The relationship between N_i and R_i [31] is described by the relation $R_i \approx \left(\frac{1}{N_i}\right)^{1/3}$. The calculated N_i and R_i are summarized in Table 2.

Table 2. The Composition, Number of Vanadium Ions Densities N_{V-ion}, Number of Lithium Ions Densities N_{Li-ion}, Vanadium Ion Spacing R_{V-ion} and Lithium Ion Spacing R_{Li-ion} for $[(90 − x) TeO_2 − (x)V_2O_5 − 10Li_2O]$ Glass Materials.

Glass Materials	$N_{V-ion} \times 10^{21}$ (cm^{-3})	$N_{Li-ion} \times 10^{21}$ (cm^{-3})	R_{V-ion} (nm)	R_{Li-ion} (nm)
$70TeO_2 − 20V_2O_5 − 10Li_2O$	6.1	18.5	54.73	37.81
$60TeO_2 − 30V_2O_5 − 10Li_2O$	8.5	17.3	49.00	38.66
$50TeO_2 − 40V_2O_5 − 10Li_2O$	10.4	15.8	45.81	39.85
$40TeO_2 − 50V_2O_5 − 10Li_2O$	12.5	15.2	43.09	40.37
$30TeO_2 − 60V_2O_5 − 10Li_2O$	14.1	14.3	41.39	41.20
$20TeO_2 − 70V_2O_5 − 10Li_2O$	15.8	13.7	39.85	41.79
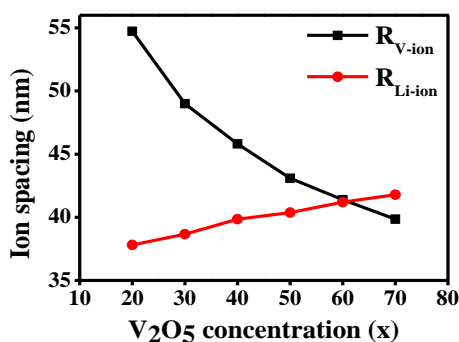
Fig. 3. The Spacing Between Vanadium and Lithium Ions as a Function of V_2O_5 Content for $[(90-x) TeO_2 − xV_2O_5 − 10Li_2O]$ Glasses.

The ion spacing for vanadium and lithium ions calculated using the values of density as shown in Fig. 3. The crossover between the values of ion spacing for vanadium and lithium takes place at the same value of x ($V_2O_5 = 60$ mol%) corresponding to the maximum of conductivity. The existence of maxima because the electronic and ionic currents combine with each other, caused by the electrostatic interactions between mobile ions and electrons (polarons). In this situation, the electronic and ionic currents are treated as independent of each other [32]. Furthermore, from the figure, it is obvious that for the domain $V_2O_5 \leq 60$ mol%, where the polaronic (electronic) conductivity dominate. In which the vanadium ion spacing decreases, and the separation between the unpaired polarons decreases. Thus, the increase in vanadium pentoxide content would increase the polaronic conductivity until reaches 60 mol%. At x = 60 mol%, the ion spacing between vanadium ions is in the range of 41 nm and for lithium ions is also about this value, as shown in the Table 2 and Fig. 3. In the domain $V_2O_5 \geq 60$ mol% the distance between

lithium ions exceeds the distance between vanadium ions, in which the glass structure becomes more open and the major formation of non – bridging oxygens increases the jump distance between vanadium hopping sites, resulting in a reduction of the conductivity [12]. In this region the number of Li^+ cations is greater than the number of V^{4+}, and therefore, the ionic conductivity becomes dominate.

The photosensitivity, an important parameter for photoconductive materials in optoelectronic devices, and it is calculated by dividing the photoconductivity σ_{ph} by the dark conductivity σ_d [33]. The value of photosensitivity has been calculated for all compositions and is given in table (1). Photosensitivity depends upon the life time of the excess charge carriers, which in turn depends upon the number of recombination centers. The higher photosensitivity in case of the glass sample $40TeO_2 – 50V_2O_5 – 10Li_2O$ indicates that the life time of excess carrier is greater in this case.

The variation of photoconductivity σ_{ph} with light intensity F has been studied at room temperature. The results for glass samples are shown in Fig. 4. It has been observed that this variation resulted in a straight line and obeys the power law given by the following equation:

$$\sigma_{ph} \, \alpha \, F^\gamma \tag{3}$$

where, σ_{ph} is the photoconductivity, F is the intensity of the light and γ is the exponent parameter and can be calculated from the slope of the straight line resulted from $\ln\sigma_{ph}$ vs. lnF curves [25]. The exponent γ is a very important parameter, which determines the recombination mechanism in the semiconductor materials. In single trap analysis [34], the value of $\gamma = 1$ corresponds to the case of monomolecular recombination, and $\gamma = 0.5$ indicates bimolecular recombination. However, when the value of γ between 0.5 and 1 cannot be supposing a series of discrete trap levels but considering the presence of a continuous distribution of localized state in the band gap, depending upon the intensity and temperature range [35]. In the present case the value of γ lies between 0.47 and 0.59 which can be considered a continuous distribution of traps exists in the band gap region with predominant bimolecular carrier recombination in the glass samples. Similar results were shown for other glass samples were reported earlier [36,37].
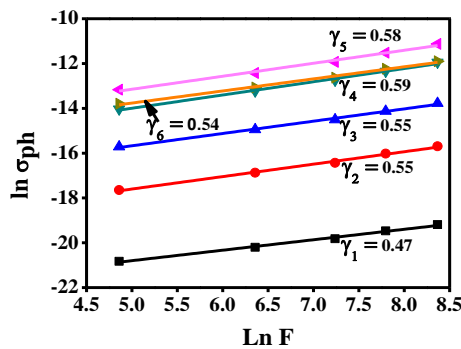
Fig. 4. Variation of Photoconductivity (σ_{ph}) with Light Intensity (F) for
[(90-x) TeO$_2$ – xV$_2$O$_5$ – 10Li$_2$O] Glass Materials.

In semiconducting glasses, upon illumination of light, electrons are excited from the valance band to the conduction band by absorbing light with the energy equal to or greater than band gap energy, leaving holes in the valance band. The holes may experience a series of capture and emission events before recombination with electrons. This leads to variation in the carrier concentration and, consequently, conductivity [38]. The conductivity change upon light absorption can proceed via two mechanisms. The carrier generation via band – to – band excitation (intrinsic), and trapping, detrapping and recombination of carriers in sub – band (imperfection or defect states) excitations (Extrinsic); photo – excited holes may be trapped by certain sub – band states leaving unpaired electrons exhibiting a long-life time. Another possible hole – trapping mechanism as discussed by Zhai et al. [39], It has been reported that in metal oxide semiconductor

nanostructures, the photoconductivity is controlled by the adsorbed oxygen molecules from the air ambient acting as trap states $(O_2 + e^- \rightarrow O_2^-)$. Under light illumination, electron-hole pairs are generated (hν → e⁻ + h⁺). The holes are attracted by the surface and recombine with negative oxygen ions on the surface $(h^+ + O_2^- \rightarrow O_2)$ leaving unpaired electrons with a long lifetime (before being trapped by re – adsorbed oxygen molecules).

The high content of transition metal oxide (TMO) in semiconducting glasses recognized to present hopping of small polarons type conduction [12]. The interaction of electron-phonon with the surrounding network supplies convenient energy for the hopping process between the transition ions sites, and the small polaronic hopping conductivity can be described by the Arrhenius relation [12]

$$\sigma = \sigma_o \exp[-E_a/k_B T] \tag{4}$$

where k_B is Boltzmann constant, E_a is the activation energy, and σ_o is the pre-exponential factor. Temperature dependence of dark and photoconductivity at intensity 2430 Lux were studied in amorphous glass samples [(90 – x) TeO$_2$ – (x)V$_2$O$_5$ – 10Li$_2$O] in the range of 300 – 400K as shown in Figs. 5,6. The conductivity in dark and in the presence of light varies exponentially with temperature according to equation (2).
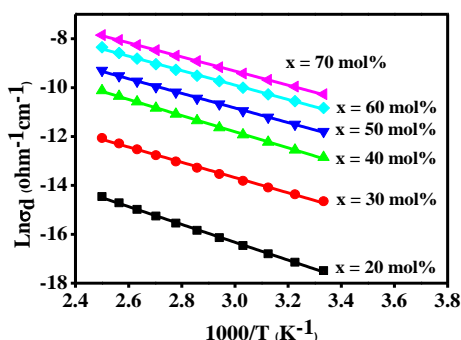
Fig. 5. Temperature Dependence of Dark Conductivity for
[(90-x) TeO₂ – xV₂O₅ – 10Li₂O], where x = 20, 30, 40, 50, 60 and 70 mol% Glass Materials.
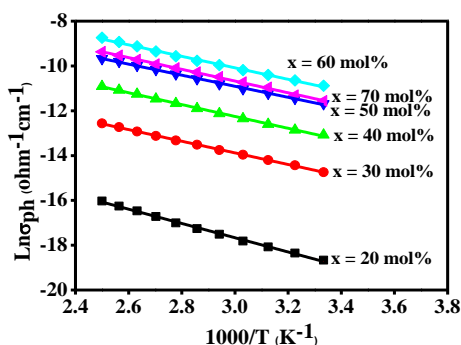
Fig. 6. Temperature Dependence of Photoconductivity for
[(90-x) TeO₂ – xV₂O₅ – 10Li₂O], where x = 20, 30, 40, 50, 60 and 70 mol% Glass Materials.

The Figs. 5& 6 indicates that, the data to be linear at the temperature range 300 – 400 K, depending on the composition. And the conduction in these glasses is through an activated process having single activation energy in this temperature range. From the slope and the intersection of the linear fitting Figs. 5,6, the values of activation energy E_a and there-exponential factor σ_o have been calculated in dark and in the presence of light, the values are listed in Table 3. The activation energy values of the discussed glasses were lying between 0.314 and 0.249 eV in dark, and in photo lie between 0.275 and 0.213 eV. The values of the activation energy of the discussed glasses

found to be smaller than as reported in the $0.5[xAg_2O - (1-x) V_2O_5 - 0.5TeO_2]$ [31], $2TeO_2 - xNa_2O - (1-x) V_2O_5$ [40], and $(0.8-x) TeO_2 - xV_2O_5 - 0.2ZnO$ [41] glassy systems. The results of dark activation energy in Table 3 indicates that, the decrease in dark activation energy E_{ad} by increasing V_2O_5 content may be related to the shift of Fermi level toward the conduction band. Also, can be explained in terms of the increased hopping conduction in the vanadium pentoxide states [42]. And, the photoactivation energy E_{ph} decrease by increasing V_2O_5 content up to 60 mol%, after that by increasing the content of V_2O_5 greater than 60 mol% the activation energy moves to higher energy. This indicates that, the defects gradually increase and move to deeper energies than that at the low content of V_2O_5 (< 60 mol%) [43].

Table 3. Results of Electrical Parameters for all Glass Samples at Intensity 2430
Lux, Applied Voltage 20 V, with Variation of Temperature from 300 – 400 K.

Glass Materials	$\sigma_{od} (\Omega^{-1}. Cm^{-1})$	E_{ad} (eV)	$\sigma_{oph} (\Omega^{-1}. Cm^{-1})$	E_{aph} (eV)
$70TeO_2 - 20V_2O_5 - 10Li_2O$	4.604×10^{-3}	0.314	3.003×10^{-4}	0.275
$60TeO_2 - 30V_2O_5 - 10Li_2O$	0.013	0.285	2.234×10^{-3}	0.243
$50TeO_2 - 40V_2O_5 - 10Li_2O$	0.150	0.269	0.013	0.228
$40TeO_2 - 50V_2O_5 - 10Li_2O$	0.155	0.258	0.030	0.221
$30TeO_2 - 60V_2O_5 - 10Li_2O$	0.360	0.255	0.091	0.213
$20TeO_2 - 70V_2O_5 - 10Li_2O$	0.525	0.249	0.0594	0.226

It is clear that from the values of E_{ach} is less than E_{ad} for all glass samples. This is due to in presence of light, the Fermi level splits into quasi-fermi levels and shifts towards the valence band for holes and towards the conduction band for electrons [44]. The position of these Fermi levels depends on light intensity. Then, in the presence of light, the band gap becomes smaller as compared to in dark [45].

The activation energy depends on the mean transition metal ions spacing (V – ions spacing R_V), as reported for other glasses [46,47]. The results of activation energy proposed that, only vanadium ions are involved in the conduction process for these glasses. The pre-exponential term as a function of the activation energy of the glasses is plotted in Fig. 7. The σ_o values were estimated from the intercept of $\ln\sigma$ vs $1000/T$ curves. The observed linear variation between $\ln\sigma_o$ and E_a indicates the presence of Meyer – Neldel rule in $[(90-x)TeO_2 - xV_2O_5 - 10Li_2O]$ glass systems. This relationship can be expressed as

$$\sigma_o = \sigma_{oo} \exp (E_a/E_{MN}) \tag{5}$$

where σ_{oo} and E_{MN} are the MN pre-exponential factor and Meyer – Neldel rule characteristic energy respectively [48,49], and are calculated from the intercept and the slope of the fitted line of $\ln\sigma_o$ vs E_a. from Fig. 7, the value of the Meyer – Neldel rule characteristic energy E_{MN} is negative is an indication of anti – Meyer – Neldel rule.
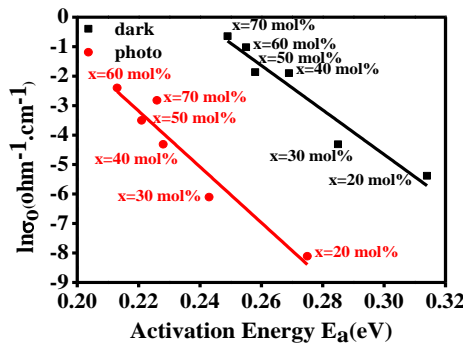
Fig. 7. Meyer – Neldel Dependence for $[(90-x) TeO_2 - (x) V_2O_5 - 10Li_2O]$ Glasses.

The difference between crystalline and amorphous semiconductor is the presence of localized states. The crystalline semiconductor is characterized by the presence on monoenergetic localized state, while an individual group of localized states is spread in the mobility gap for the amorphous and glassy semiconductor [50]. Transient photoconductivity supplies information about the defect of states distribution, the carrier life time, the recombination and the trapping mechanism, by studying rise and decay of photocurrent I_{ph} with the development of time by exposing the glass samples to visible light. After a certain time of exposure (beginning of illumination), the growing of photogenerated charge carrier become remarkable and starts filling the traps until the generation rate comes close to the recombination rate [51]. After that the light was turned off, the generation of photocarrier stopped while the recombination of trapped carrier continues leads to decay in photocurrent [51]. Therefore, the decay rate of photocurrent determines the carrier life time existing in the trap states. The initial dark value of current was subtracted to obtain photocurrent I_{ph} during rising and decay. Different behaviors in transient photoconductivity for chalcogenide glasses were observed, such as, a maximum was detected in the growing of photocurrent [52], and no maxima were observed in some compositions of chalcogenide glass [51].

To study the transient photoconductivity behavior in $[(90 - x) TeO_2 - (x)V_2O_5 - 10Li_2O]$ glass materials, we performed three sets of measurements for the rise and decay of photocurrent at different intensities, temperatures and applied voltages. Photocurrent rise and decay measurements have been made on $[(90 - x) TeO_2 - (x)V_2O_5 - 10Li_2O]$ glass materials with the exposure time at room temperature at different illumination light intensities (129 – 8730 lux). Fig. 8 shows the variation of photocurrent with the time of illumination, as the light is switched on, the photocurrent rises monotonically with time until reaches saturation. While, after switching off the light, the decay of photocurrent is fast in the beginning and become quite slow, found that the decay of photocurrent is non – exponential. This behavior is similar for all studied light intensities, and all the glass samples show a similar trend by increasing V_2O_5 content. The same behavior has already been observed in other glasses [53,54]. However, in the present case, the photocurrent decay curves don't have the same slope, which decreases continuously with time. This indicates that, different kinds of traps exist at different energies in the band gap. These traps have different time constants and give the non – exponential decay. In the case of a single trap level, the decay curve must be a straight line [42]. Bube [34] reported that, in amorphous materials having traps in the band gap, when the free carrier density is more than the trapped carrier density, then the recombination time of carriers is the same as the carrier lifetime. If the carrier density is less than the trapped carrier density, then the recombination process is controlled by the rate of trap emptying and is larger than the carrier lifetime, resulting in a slow decay [42].

The photocurrent decay for the $[(90 - x) TeO_2 - (x)V_2O_5 - 10Li_2O]$ glass materials can be explained using Street and Mott model [52] for the dangling bond levels. Suggested that, the recombination mechanism is through the metastable neutral defects D^0 (neutral dangling bonds) centers under nonequilibrium steady state conditions. But the chalcogenide materials having charged defect $D^{+ (-)}$ over the neutral defect D^0 under equilibrium conditions. This means that, the negatively charged defects D^- and the positively charged defects D^+ have a distributed level in the gap around the Fermi level, that pin the Fermi level near the middle of the gap. Under illumination, the optically excited electron trapped in the D^+ level and transformed to D^0 level by the reaction $D^+ + e \rightarrow D^0$. This electron from the neutral center can recombine with the trapped hole in D^- level by the reaction $D^- + h \rightarrow D^0$, or emitted into the conduction mechanism. Therefore, the number of photocarriers is proportional to the excess density of D^0 defects. Then the recombination mechanism takes place via trapped electron and hole in D^+ and D^- levels respectively. Which called bimolecular recombination $(2D^0 \rightarrow D^+ + D^-)$. Then, at the beginning of illumination there is a sharp increase in photocurrent intensity followed by saturation, and after turning off the exposing light, the photocurrent decreases gradually due to the bimolecular recombination.

Fig. 8 shows the slow increase in photocurrent intensity with vanadium pentoxide content until reach 60 mol%. This can have related to the change in the trap density of states for the studied amorphous glass. In which, some extra electrons supply to D^+ states by increasing V_2O_5 content, then part of D^+ states transformed into D^0 states. For this reason, the equilibrium between

the photo generated charge carriers and its trapping in defect states are retarded, due to the decreased density of D^+ state, leading to the slow increase in the photocurrent [51]. Also, the photocurrent is saturated at a low light intensity, while by increasing the intensity of light exposure, the photocurrent not saturated as shown in Fig. 6. This is due to the excess photo-generated charge carriers due to the increased light intensity participated in the conduction. That reflects the no availability of vacant trap states for excess photo generated charge carriers, which leads to the delay of saturation of photocurrent [51]. Also, in Fig. 8 shows the decay of photocurrent initially is fast, this is referred to the direct recombination of charge carriers with opposite sign carriers, and the slow decay due to bimolecular recombination [51].
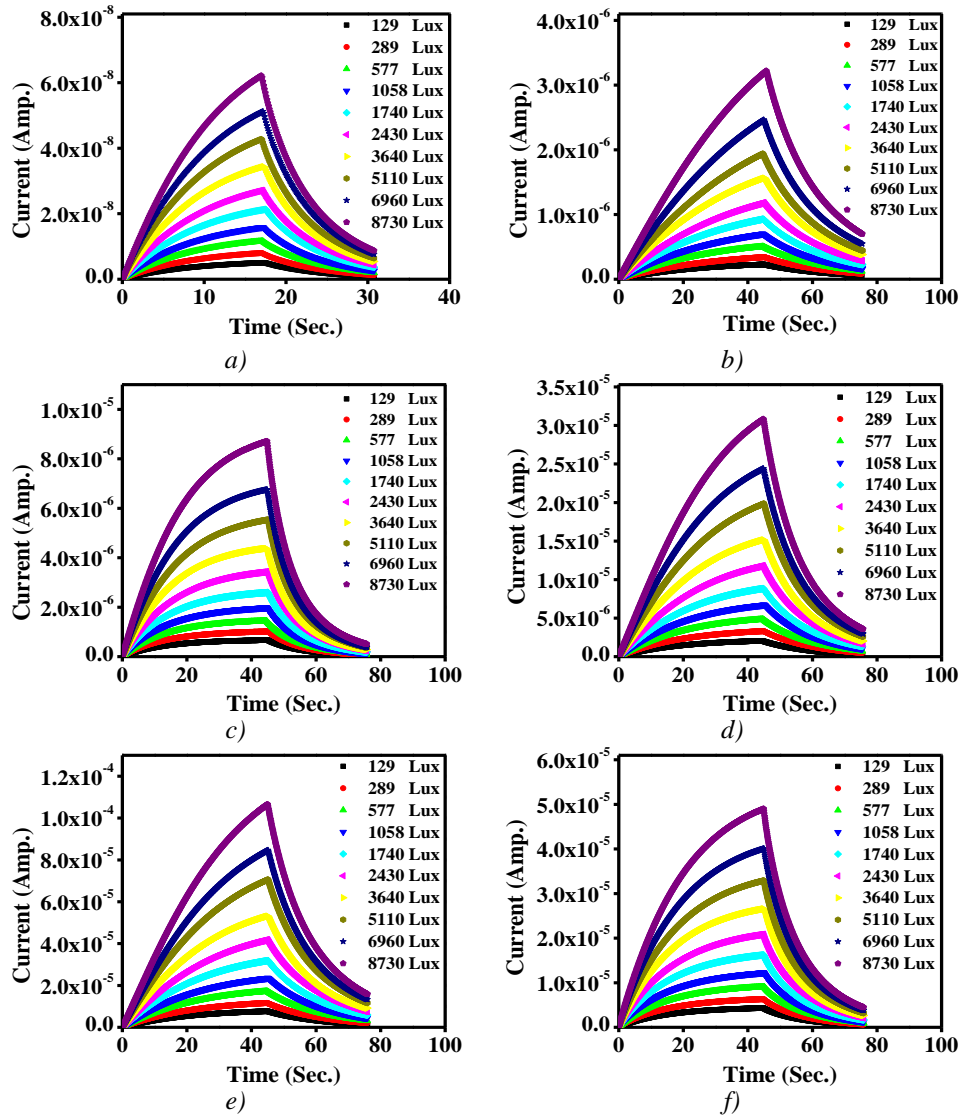
Fig. 8. Rise and Decay of Photocurrent with Time at Different Light Intensities for (a) $70TeO_2 – 20V_2O_5 – 10Li_2O$, (b) $60TeO_2 – 30V_2O_5 – 10Li_2O$, (c) $50TeO_2 – 40V_2O_5 – 10Li_2O$, (d) $40TeO_2 – 50V_2O_5 – 10Li_2O$, (e) $30TeO_2 – 60V_2O_5 – 10Li_2O$, (f) $20TeO_2 – 70V_2O_5 – 10Li_2O$ Glass Materials.
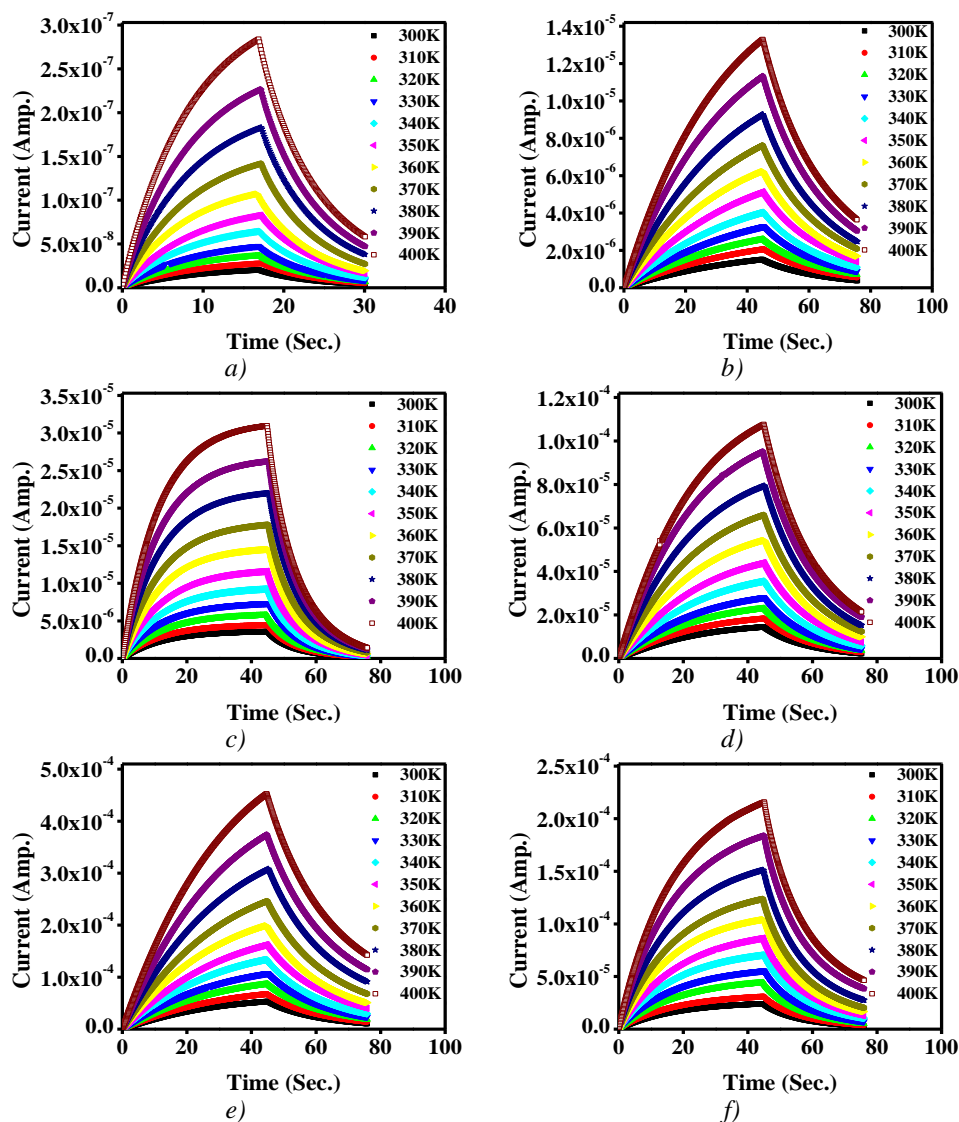
Fig. 9. Rise and Decay of Photocurrent with Time at Different Temperatures for
a) $70TeO_2 – 20V_2O_5 – 10Li_2O$, (b) $60TeO_2 – 30V_2O_5 – 10Li_2O$, (c) $50TeO_2 – 40V_2O_5 – 10Li_2O$, (d) $40TeO_2 –$
$50V_2O_5 – 10Li_2O$, (e) $30TeO_2 – 60V_2O_5 – 10Li_2O$, (f) $20TeO_2 – 70V_2O_5 – 10Li_2O$ Glass Materials.

Another set of measurements was made at different temperatures from 300 K to 400 K keeping the illumination intensity is constant at 2430 lux. The rise and decay of photocurrent for the glass samples is shown in Fig. 9. In this case, the behavior of the rise and decay curves is similar at different intensities. From the figures the magnitude of the photocurrent increases by increasing the temperature [300 – 400 K] and also increases by increasing the concentration of V_2O_5 up to 60 mol% after that the value of current decreases by increasing V_2O_5 content exceed than 60 mol%. The behavior of rising and decay curves of photocurrent is similar at different temperatures for the studied glass materials, the third set of measurements has been taken at different applied voltages at room temperature and light intensity 2430 lux. The rise and decay of photocurrent for the glass samples was shown in Figs. (10). Same results shown in these figures by effect of the applied voltage to the glass samples as compared to the other measurements (effect of intensity and temperature), the magnitude of the photocurrent is higher in sample $30TeO_2 – 60V_2O_5 – 10Li_2O$ as compared to other samples, and the photocurrent increases with the increase in applied voltage [10 – 100V].
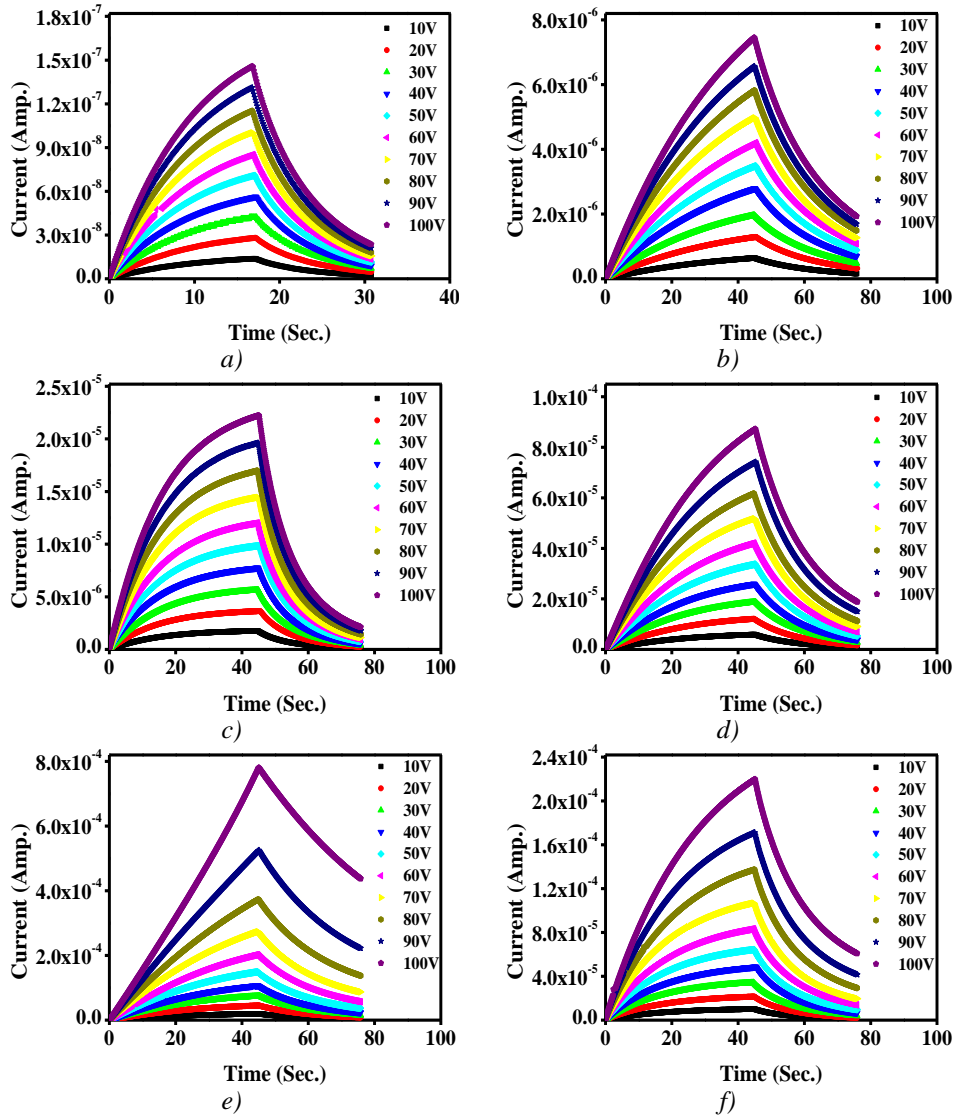
Fig. 10. Rise and Decay of Photocurrent with Time at Different Applied Voltages for
a) $70TeO_2 - 20V_2O_5 - 10Li_2O$, (b) $60TeO_2 - 30V_2O_5 - 10Li_2O$, (c) $50TeO_2 - 40V_2O_5 - 10Li_2O$, (d) $40TeO_2 -$
$50V_2O_5 - 10Li_2O$, (e) $30TeO_2 - 60V_2O_5 - 10Li_2O$, (f) $20TeO_2 - 70V_2O_5 - 10Li_2O$ Glass Materials.

The behavior of rising and decay curves is similar at different applied voltages. Fig. (10) shows also at the glass material $30TeO_2 - 60V_2O_5 - 10Li_2O$ when the applied voltage is much higher (exceed 80 volt), the photocurrent may not be proportional to the applied voltage due to increase in charge carriers at higher applied voltages. the photocurrent becomes super-ohmic at these voltages. this type of behavior is possible because injection of the charge from the electrodes at the higher voltages which is known as space charge limited conduction [55].

To analyze the decay rates in case of non − exponential decay, we use the concept of a differential life time (decay time constant) as described by Fuhs and Meyer [56], using the relation

$$\tau_d = - \left[\frac{1}{I_{ph}} \frac{dI_{ph}}{dt} \right]^{-1}$$

(6)

where I_{ph} is the photocurrent when the light is switched off, and $\left(\frac{dI_{ph}}{dt} \right)$ is the decay rate.

In the case of exponential decay, the differential life time should not vary with time and equal to carrier life time. In case of non – exponential decay τ_d will increase with time and only the value t = 0 will correspond to carrier life time.

Fig. 11a shows the variation of τ_d with time at room temperature and different light intensities for $70TeO_2 - 20V_2O_5 - 10Li_2O$ glass sample. It is clear from the figure that, the decay time constant τ_d increases with increasing time, which confirms the non – exponential decay of photocurrent. Then, the glass sample has free carrier densities higher than the trapped carrier density by increasing in the time of light intensity. By increasing the concentration of V_2O_5 the number of defect centers increases, motivated more localized states, which plays a role as trapping centers. These traps store the charge carriers (electrons and holes), for this reason the recombination rate is delayed, corresponding to the differential life time is increased by increasing V_2O_5 content. The same behavior of the variation of a differential life time with time shown in Fig. (11(b-c)) by the variation of temperature and applied voltage.

Fig. 12a shows the plot of τ_d versus "x" the V_2O_5 concentration, at room temperature and different light intensities. The value of τ_d first increases (up to x = 40 at%) and then decreases (from x = 50 at% to 60 at %) as the concentration of V_2O_5 increases. After that τ_d increases by increasing V_2O_5 concentration greater than 60 at%. The higher value of τ_d in $50TeO_2 - 40V_2O_5 - 10Li_2O$ glass material, indicates the slower decay and hence an increased value of the density of localized state in the mobility gap. The same results also are shown in Fig. 12(b-c) by the variation of temperature and applied voltage.
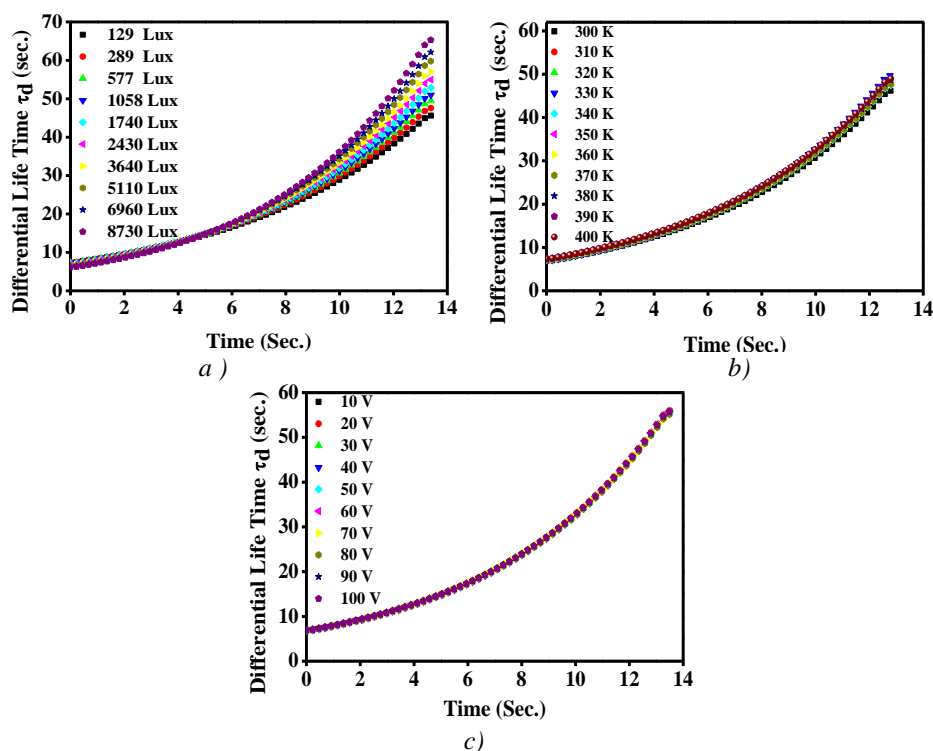
Fig. 11. Variation of Differential Life Time with Time at: (a) Different Light Intensities, (b) Different Temperatures and (c) Different Applied Voltages for $70TeO_2 - 20V_2O_5 - 10Li_2O$ Glass Material.
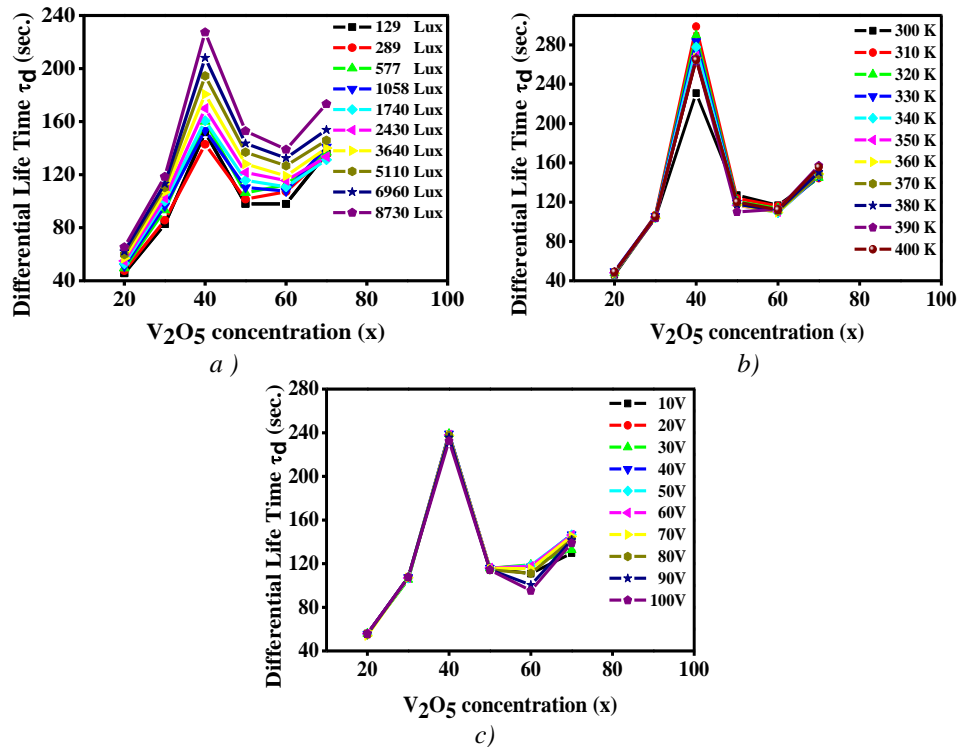
Fig. 12. Variation of Differential Life Time with V_2O_5 Concentration at: (a) Different Light Intensities, (b) Different Temperatures and (c) Different Applied Voltages for 70 TeO_2 – 20 V_2O_5 – 10Li_2O Glass Material.

4. Conclusion

The glass (90 – x) TeO_2 – (x) V_2O_5 – 10Li_2O in mol% samples were prepared by using a rapid quenching method. The steady photocurrent density of the present samples, that were prepared by rapid quenching technique, shows an ohmic nature. The photocurrent increased with rising light intensity and reach a maximum at 60 mole% of vanadium pentoxides. Moreover, the highest photosensitivity was observed at x= 50 mol% due to the greater of the lifetime of the excess carrier. The photoactivation energy increased up to x=60 mole%, therefore, the 30TeO_2-60 V_2O_5-10Li_2O in mol% can be used for optoelectronic devices. The non-exponential decay is dependent on the time and the light intensity.

References

[1] M. Sathish, B. Eraiah, Materials Science and Engineering **73**, 012137 (2015).
[2] G. Ori, M. Montori, A. Pedone, C. Siligardi, Journal of Non – Crystalline Solids **357**, 2571 (2011).
[3] R. V. Barde, S. A. Waghuley, Journal of Advanced Ceramics **2**(3), 246 (2013).
[4] El Sayed Yousef, A. E. Al-Salami, M. Hotzel, Bulletin of Materials Science **35**(6), 961 (2012).
[5] El Sayed Yousef, H. H. Hegazy, M. M. Elokr, Y. M. Aboudeif, Chalcogenide Letters **12**(12),

653 (2015).

[6] M. Irannejad, Z. Zhao, B. Richards, G. Jose, A. Jha, T. Fernandez, P. Joshi, J. Lousteau, International Journal of Applied Glass Science **4**(3), 202 (2013).

[7] N. F. Mott, E. A. Davis, Oxford, 2nd Edition (2012).

[8] B. Sujatha, R. Viswanatha, H. Nagabushana, C. N. Reddy, Journal of Materials Research and Technology **6**, 7 (2017).

[9] A. Rajiv, M. S. Reddy, R. Viswanatha, J. Uchil, C. N. Reddy, Bulletin of Materials Science **38**(4), 985 (2015).

[10] N. A. Szreder, P. Kosiorek, J. Karczewski, M. Gazda, R. J. Barczyński, Procedia Engineering **98**, 62 (2014).

[11] R. Hisam, A. K. Yahya, H. M. Kamari, Z. A. Talib, Ionics **23**, 1423 (2017).

[12] S. A. Salehizadeh, B. M. G. Melo, F. N. A. Freire, M. A. Valente, M. P. F. Graça, Journal of Non – Crystalline Solids **443**, 65 (2016).

[13] R. Zheng, X. Zhou, Y. Yang, Q. Wu, P. Lv, K. Yu, W. Wei, Journal of Non – Crystalline Solids 471, 280 (2017).

[14] A. Chatterjeea, A. Ghosh, AIP Conference Proceedings **1942**, 070030 (2018).

[15] J. Nikolić, L. Pavić, A. Šantić, P. Mošner, L. Koudelka, D. Pajić, A. Moguš-Milanković, Journal of the American Ceramic Society **101**, 1221 (2018).

[16] L. Li, M. Li, I. M. Reaney, D. C. Sinclair, Journal of Materials Chemistry C **6300**, 5 (2017).

[17] D. Souri, Z. E. Tahan, S. A. Salehizadeh, Indian Journal of Physics **90**, 407 (2016).

[18] S. Laila, A. K, Suraya, A. K, Yahya, Chalcogenide Letters **11**(2), 91 (2014).

[19] E. E. Assem, I. Elmehasseb, Journal of Materials Science **46**, 2071 (2011).

[20] G. D. L. K. Jayasinghe, M. A. K. L. Dissanayake, P. W. S. K. Bandaranayake, J. L. Souquet, D. Foscallo, Solid State Ionics **121**, 19 (1999).

[21] R. A. Montani, M. A. Frechero, Solid State Ionics **177**, 2911 (2006).

[22] N. Krins, A. Rulmont, J. Grandjean, B. Gilbert, L. Lepot, R. Cloots, B. Vertruyen, Solid State Ionics 177, 3147 (2006).

[23] R. K. Pal, S. Yadav, A. K. Agnihotri, A. Kumar, Chalcogenide Letters **7**(10), 587 (2010).

[24] S. Shukla, S. Kumar, Bulletin of Materials Science **34**(7), 1351 (2011).

[25] N. Chaudhary, A. A. Bahishti, M. Zulfequar, Physica B **407**, 2267 (2012).

[26] Seema Dalal, S. Khasa, M. S. Dahiya, A. Agarwal, A. Yadav, V. P. Seth, S. Dahiya, Materials Research Bulletin **70**, 559 (2015).

[27] K. Sega, A. Kassai, H. Sakata, Materials Chemistry and Physics **53**, 28 (1998).

[28] R. Singh, J. S. Chakravarthi, Physical Review B **55**(9), 5550 (1997).

[29] P. Jowzwiak, J. E. Garbarczyk, Solid State Ionics **176**, 2163 (2005).

[30] L. Bih, M. E. Omari, J. M. Reau, A. Nadiri, A. Yacoubi, M. Haddad, Materials Letters **50**, 308 (2001).

[31] H. M. M. Moawad, H. Jain, R. El-Mallawany, Journal of Physics and Chemistry of Solids **70**, 224 (2009).

[32] J. E. Garbarczyk, P. Machowski, M. Wasiucionek, W. Jakubowski, Solid State Ionics **157**, 269 (2003).

[33] R. K. Pal, S. Yadav, A. K. Agnihotri, D. Kumar, A. Kumar, Journal of Non-Oxide Glasses **1**, 285 (2009).

[34] R. H. Bube, "Photoconductivity of Solids", Wiley, New York, 1960.D.

[35] A. Rose, "Concept in Photoconductivity", Interscience, New York, 1963.

[36] A. Thakur, V. Sharma, P. S. Chandel, N. Goyal, G. S. S. Saini, S. K. Tripathi, Journal of Material Science **41**, 2327 (2006).

[37] S. Shukla, S. Kumar, Chalcogenide Letters **6**, 695 (2009).

[38] M. Mousavi, Sh. T. Yazdi, Modern Physics Letters B **30**, 1650151 (2016).

[39] T. Zhai, X. Fang, M. Liao, X. Xu, H. Zeng, B. Yoshio, D. Golberg, Sensors **9**, 6504 (2009).

[40] G. D. L. K. Jayasinghe, M. A. K. L. Dissanayake, M. A. Careem, J. L. Souquet, Solid State Ionics **93**, 219 (1997).

[41] R. Singh, J. S. Chakravathi, Physical Review B **55**, 5550 (1997).

[42] Vineet Sharma, J. Optoelectron. Adv. M. **8**(5), 1823 (2006).

[43] S. V. Kondratenko, O. V. Vakulenko, Yu. I. Mazur, V. G. Dorogan, E. Marega, Jr., M.

Benamara, M. E. Ware, G. J. Salamo, Journal of Applied Physics **116**, 193707 (2014).
[44] Kumar, S. Kumar, Turkish Journal of Physics **29**, 91 (2005).
[45] S. K. Tripathi, V. Sharma, A. Thakur, J. Sharma, G. S. S. Saini, N. Goyal, Journal of Non – Crystalline Solids **351**, 2468 (2005).
[46] D. Souri, Journal of Non – Crystalline Solids **356**, 2181 (2010).
[47] N. Vedeanu, O. Cozar, I. Ardelean, B. Lendl, D. A. Magdas, Vibrational Spectroscopy **48**(2), 259 (2008).
[48] K. Singh, N. Mehta, S. K. Sharma, A. Kumar, Processing and Application of Ceramics **10**(3) 137 (2016).
[49] A. Kumar, N. Mehta, Journal of Physics and Chemistry of Solids **121**, 49 (2018).
[50] R. K. Pal, A. K. Agnihotri, A. Kumar, Chalcogenide Letters **7**(6), 439 (2010).
[51] Ravi Chander, R. Thangaraj, Applied Physics A **114**, 619 (2014).
[52] N. Kushwaha, V. S. Kushwaha, R. K. Shukla, A. Kumar, Journal of Non – Crystalline Solids **351**, 3414 (2005).
[53] S. Shukla, S. Kumar, AIP Conference Proceedings **1349**, 513 (2011).
[54] M. Ashraf, S. El Yousef, S. Almoeed, ournal of Ovonic Research **13**, 315 (2017).
[55] S. Yadav, S. K. Sharma, A. Kumar, Journal of Alloys and Compounds **509**, 6 (2011).
[56] R. Sathyamoorthy, P. Sudhagar, S. Chandramohan, K. P. Vijayakumar, Crystal Research & Technology **42**(5), 498 (2007).